Optics Letters

Temporal correlations imaging fixed targets through turbulence

Damián Gulich[1,2]

[1]Instituto de Física de Líquidos y Sistemas Biológicos, CONICET, UNLP, Calle 59 Nro. 789, 1900 La Plata, Argentina
[2]Departamento de Ciencias Básicas, Facultad de Ingeniería, Universidad Nacional de La Plata (UNLP), 1900 La Plata, Argentina (dgulich@iflysib.unlp.edu.ar)

Received 16 February 2016; revised 10 May 2016; accepted 27 May 2016; posted 27 May 2016 (Doc. ID 259578); published 15 June 2016

We study the temporal correlations from dynamic imaging through turbulence using incoherent light from fixed high-contrast targets. We conduct our experiment in controlled laboratory conditions using several values of the C_n^2 constant from the weak to strong fluctuation regime. We employ *detrended fluctuation analysis* to measure long-range correlations while considering scintillation information for every recorded pixel. We find that turbulence strength generally increases temporal correlations in time series from pixels in high-contrast regions of the image.

OCIS codes: (000.5490) Probability theory, stochastic processes, and statistics; (010.1290) Atmospheric optics; (010.1300) Atmospheric propagation; (010.1330) Atmospheric turbulence; (010.7060) Turbulence; (070.2025) Discrete optical signal processing.

http://dx.doi.org/10.1364/OL.41.002855

The existence of spatial and temporal fluctuations in air produces index-of-refraction variations that deform optical waves propagating through this turbulent medium. In imaging experiments, this phenomenon produces a dynamic blur in formed images and is generally known as *seeing* [1]. Since McGlamery's original paper [2] addressing the simulation of an optical wave propagating through turbulence, several methods have been proposed to incorporate the temporal dynamics of the process [3,4], and cited references. However, experimental work usually focuses on thin beam [5,6] or average beam dynamics [7,8]. In a previous work [9], we proposed an inexpensive setup for the dynamic incoherent imaging of fixed (high-contrast) targets through turbulence; in this Letter, we investigate the presence of long-term memory effects in that same experimental setup.

For the purpose of estimating the temporal correlations present in this imaging situation (to later find their relation with known turbulence intensity) we will use *detrended fluctuation analysis* (DFA). The DFA technique is widely used to characterize the fractal dynamics of a system from which a time series has been measured [10], and it is the most popular approach to detect the presence of long-term memory in data [11]. However, specific applications in the optical field are scarce [6,12–15]. In this Letter, we propose to characterize temporal correlations by imaging fixed targets through atmospheric turbulence by means of a pixel-by-pixel DFA estimation of the Hurst exponent (H).

The DFA method follows five steps that we shall briefly enumerate (the reader will find a more detailed explanation in Refs. [16,17]). Step 1: given a time series $S = \{x_t, t = 1, \ldots, N\}$, with N being the number of equidistant observations, the cumulated data series $Y(k) = \sum_{t=1}^{k}(x_t - \langle x\rangle)$, with $k = 1, \ldots, N$ and $\langle x\rangle = (\sum_{t=1}^{N} x_t)/N$, is considered. Step 2: this profile is divided into $\lfloor N/s\rfloor$ nonoverlapping windows of equal length s ($\lfloor a\rfloor$ denotes the largest integer less than or equal to a). Step 3: a local polynomial fit $y_{\nu,m}(k)$ of degree m is fitted to the profile for each window $\nu = 1, \ldots, \lfloor N/s\rfloor$. The degree of the polynomial can be varied to eliminate constant ($m = 0$), linear ($m = 1$), quadratic ($m = 2$), or higher order trends of the profile. Step 4: the variance of the detrended time series is evaluated by averaging over all data points k in each segment ν, $F_m^2(\nu, s) = (1/s)\sum_{k=1}^{s}\{Y[(\nu - 1)s + k] - y_{\nu,m}(k)\}^2$, for $\nu = 1, \ldots, \lfloor N/s\rfloor$. Step 5: the DFA fluctuation function is obtained by averaging over all segments and taking the square root, $F_m(s) = \{(1/\lfloor N/s\rfloor)\sum_{\nu=1}^{\lfloor N/s\rfloor}[F_m^2(\nu, s)]\}^{1/2}$. This procedure should be repeated for different values of the time scale s in order to unveil the s-dependence of F_m. If the time series has long-range power-law correlations, $F_m(s)$ scales as

$$F_m(s) \sim s^H, \tag{1}$$

for a certain range of s [18]. The Hurst exponent for a given pixel, H, is estimated by the slope of the best linear regression in a double logarithmic plot. The long-range correlations embedded in the time series are quantified by this exponent: if $H > 1/2$, consecutive increments tend to have the same sign so that these processes are *persistent*. If $H < 1/2$ consecutive increments are more likely to have opposite signs, and it is said that the processes are *antipersistent*. $H = 1/2$ is obtained for uncorrelated data [19].

Since in this Letter we deal with dynamic imaging of a fixed target through turbulence, we will have an intensity time series $I_{i,j}(t)$ for each recorded pixel, and the DFA method will provide a pixel-based Hurst exponent $H_{i,j}$. Considering the individual irradiance of a single pixel we defined in [9] the *pixel-based scintillation index* $(\sigma_I^2)_{i,j}$:

$$(\sigma_I^2)_{i,j} = \frac{\langle I_{i,j}^2 \rangle}{\langle I_{i,j} \rangle^2} - 1, \quad (2)$$

where $I_{i,j}(t)$ expresses the irradiance over time of an image pixel with coordinates (i, j) given by an optical wave propagating through an active atmospheric turbulence and $\langle\,\rangle$ is the time average. For incoherent imaging through atmospheric turbulence, the intensity of a target image (at the receivers' aperture) will fluctuate the most on high-contrast borders [20] and will barely fluctuate over uniform regions; therefore, the visual representation of $(\sigma_I^2)_{i,j}$ will resemble an edge-filter applied to the target image [21]. In order to locate only the pixels with a relatively high scintillation, where most of turbulence information is located for this situation [9], a threshold value τ can be applied to this scintillation index representation to define a binary set $\Omega_{i,j} = \{0 \text{ if } (\sigma_I^2)_{i,j} < \tau, \text{ and } 1 \text{ if } \tau \le (\sigma_I^2)_{i,j} < 1\}$ (pixels related to edges of highest contrast over the imaged target). In [9] we found that the amount of nonzero pixels in $\Omega_{i,j}$ can be compared to the amount of nonzero pixels from a simple binary edge detection filter output $E_{i,j}$ applied to the time-average image [21]. The relationship between these magnitudes in our experimental setup was found to be

$$\sum_{i,j} \Omega_{i,j} = \left(\sum_{i,j} E_{i,j} \right) \frac{C_n^2}{G_0}, \quad (3)$$

where $G_0 = (2.39 \pm 0.08) \cdot 10^{-8}$ m$^{-2/3}$. This result shows that (a) the number of high scintillation pixels increases with turbulence intensity with respect to the amount of edge pixels in the mean image; (b) these pixels are located in high-contrast regions of target image; and (c) turbulence intensity information is preserved in $\sum_{i,j} \Omega_{i,j}$.

In order to study $H_{i,j}$ values as a function of C_n^2, we performed a conceptually simple experiment of laboratory imaging in controlled conditions in which a checkerboard pattern [Fig. 2(a)] is displayed on a standard LCD monitor followed by a region with an artificial turbulence (depicted in Fig. 1) and then focused on an off-the shelf webcam (Logitech Webcam Pro 9000, 640 × 400 resolution, 30 frames/s).

For the purpose of having a fully developed inertial turbulence at stable and statistically repeatable conditions, we employ a laboratory turbulent chamber commonly called a turbulator [22,23]. To simulate the atmospheric turbulence, two air fluxes at different temperatures are forced to collide in the chamber, producing an isotropic mix between hot and cold air. The heat source is an electric heater controlled by changing the current passing through it, and the cold channel injects room-temperature air. Light from the target propagates across ∼0.35 m of turbulence in the mixing chamber. The strength of the artificial turbulence, quantified by the refractive index structure constant C_n^2, and the inner and outer scales (l_0 and L_0) were previously estimated following the procedure suggested by Masciadri and Vernin [24] ($l_0 \sim 3$ mm and $L_0 \sim 15$ cm). Particularly, C_n^2 is expressed as a function of the temperature difference between hot and cold sources ($\Delta T = T_1 - T_2$). Experiments were carried out with 13 temperature differences ranging from 15.5°C to 152.7°C, all with characterized C_n^2 ranging from $9.54 \cdot 10^{-9}$ to $3.99 \cdot 10^{-8}$ m$^{-2/3}$ and calculated Rytov variance σ_R^2(632 nm) ranging from 0.24 to 1.02 (weak to strong fluctuation range [8]). Reference measurements with the fans on and off were captured as well and can be considered

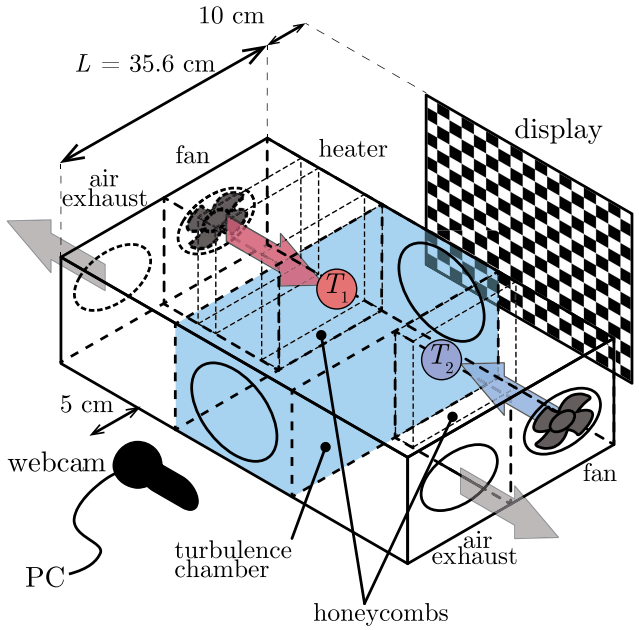

Fig. 1. Experimental setup. The turbulator is suspended from an independent structure in order to avoid any vibration in optical components.

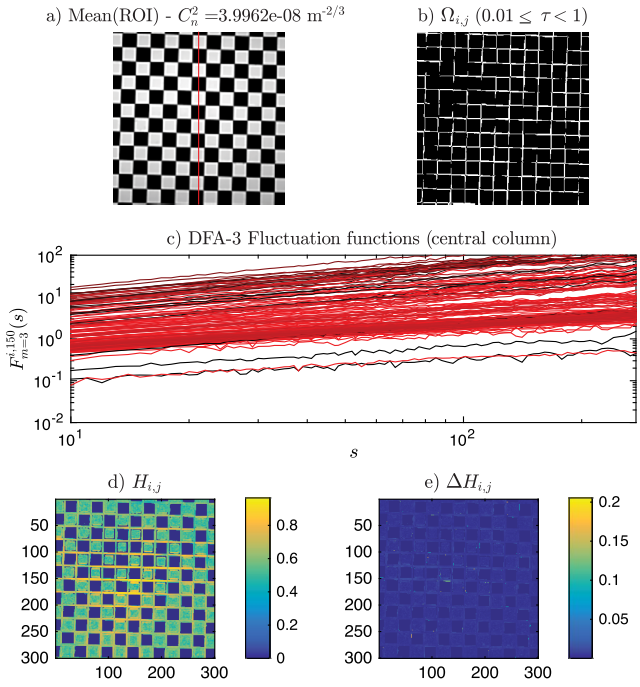

Fig. 2. Representative case, strongest turbulence condition ($C_n^2 \sim 4 \cdot 10^{-8}$ m$^{-2/3}$). (a) Average frame of checkerboard in ROI (300 × 300 pixels) affected by turbulence (300 pixels ≡ 15.027 cm); the red line (central column) is detailed in -c. (b) Visual representation of $\Omega_{i,j}(\tau = 0.01)$; (c) fluctuation functions for pixels in the middle column of -a (red line): lines go from black to red based on mean image value pixel (black for the darkest, and red for the brightest). (d) Visual representation of $H_{i,j}$; (e) error $\Delta H_{i,j}$ in the estimation of $H_{i,j}$ (note that all values are one order of magnitude smaller than $H_{i,j}$).

as background measurements to quantify the electronic, mechanical noise and room turbulence effects.

We determined a region of interest (ROI) of 300 × 300 pixels (300 pixels ≡ 15.027 cm). We selected the green channel from the RGB output of the camera ($\lambda \sim 510$ nm) for analysis purposes. Averages were taken for 1100 consecutive frames (~36.7 s) [see Fig. 2(a)].

For the DFA analysis, we chose a detrending polynomial of degree $m = 3$ (this is customary; however we have tried $m = 1$ and 2 with similar results), and estimated the fluctuation functions for 100 scale sizes $10 \leq s \leq 275$. A representative case is depicted in Fig. 2. We chose the full range of scales s to fit all fluctuation functions. This interval choice is both supported by the resulting ~10% uncertainty in slope (H) estimations [Fig. 2(e)] and a range estimation criterion described in [18] for several randomly selected fluctuation functions. It is worth noting that, for all studied turbulence intensities, in the visual representation of $H_{i,j}$ [Fig. 2(d)], the values of $H_{i,j} \sim 0$ (<1/2, antipersistent) correspond to extremely low intensity target pixels (homogeneous black areas), where even the noise level becomes too low for this setup. In extremely high intensity target pixels (homogeneous white areas) we observe predominantly $H_{i,j} \sim 1/2$ (uncorrelated): fluctuations in these areas are mainly due to electronic noise. Values of $H_{i,j} > 1/2$ (persistent) are observed within high-contrast edges of the target, which are known to have high scintillation [Fig. 2(b)]; we shall therefore focus the study on Hurst exponents H in Ω (we now drop the subindices for notation simplicity).

We studied the distributions of H values in Ω for references and all experimental cases and found that the mean and standard deviation are representative of the set. Both references H means in Ω are around 1/2 (uncorrelated data), and are predominantly attributable to electronic noise (mechanical noise effect is negligible). With these histogram considerations, we can now study the behavior of mean H in $\Omega(\bar{H}_\Omega)$ as a function of C_n^2 (please refer to Fig. 3). Observed correlations generally increase with C_n^2 with a maximum observed mean $\bar{H}_\Omega = 0.7 \pm 0.1$. We find that in ranges explored experimentally in this Letter $\bar{H}_\Omega$, as a first approximation, scales according to

$$\bar{H}_\Omega \sim \frac{C_n^2}{C_H} + H_0, \tag{4}$$

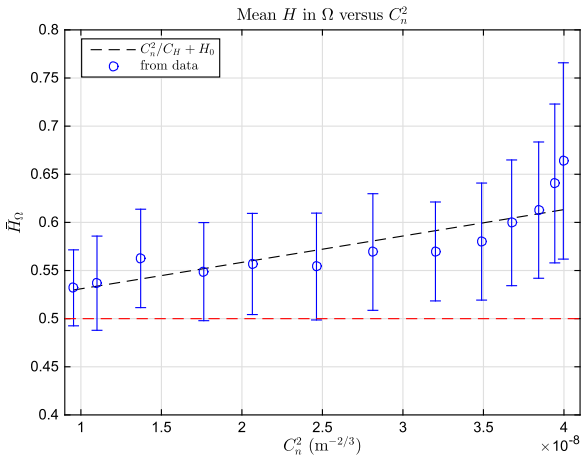

Fig. 3. Mean H in Ω as a function of C_n^2 (error bars are from the std(H) in that set); the linear approximation (black dashed line) has $R^2 = 0.7426$. The red dashed line indicates $H = 1/2$ (uncorrelated).

Table 1. Summary of Results

	Estimated Value
C_H	$(3.6 \pm 1.4) \cdot 10^{-7}$ m$^{-2/3}$
H_0	0.50 ± 0.03

where $C_H = (3.6 \pm 1.4) \cdot 10^{-7}$ m$^{-2/3}$ and $H_0 = 0.50 \pm 0.03$ (these results are summarized in Table 1). This value of H_0 emphasizes the fact that scintillating pixels in low turbulence conditions (in this setup) are mostly affected by electronic noise, as expected from previous remarks.

In summary, we have found that when imaging a high-contrast target through turbulence, correlations increase with turbulence intensity for pixels with a relative high scintillation index. This knowledge may be key to refine the temporal aspect for both simulation techniques and theoretical models. Imaging simulation techniques should take into account restrictions in output pixel time series imposed by Eqs. (3) and (4); moreover, we have found that both are linearly related to C_n^2 in our experimental range. The general study of $H_{i,j}$ conducted in this Letter may also benefit the field of image reconstruction in turbulence conditions: for observed pixels with $H_{i,j} < 1/2$ (antipersistent) consecutive increments in the time series are more likely to have opposite signs, so that taking the temporal average becomes statistically representative of the actual target value. However, pixels found to have greater $H_{i,j}$ values must be dealt with other reconstruction techniques. This problem will be studied in future communications.

Funding. Consejo Nacional de Investigaciones Científicas y Técnicas (CONICET); Universidad Nacional de La Plata (UNLP).

Acknowledgment. The author thanks Luciano Zunino for his helpful review of the Letter.

REFERENCES

1. L. C. Andrews and R. L. Phillips, *Laser Beam Propagation through Random Media*, 2nd ed. (SPIE, 2005).
2. B. L. McGlamery, J. Opt. Soc. Am. **57**, 293 (1967).
3. H. Jakobsson, Appl. Opt. **35**, 1561 (1996).
4. B. M. Welsh, Proc. SPIE **3125**, 327 (1997).
5. G. Funes, D. Gulich, L. Zunino, D. G. Pérez, and M. Garavaglia, Opt. Commun. **272**, 476 (2007).
6. L. Zunino, D. Gulich, G. Funes, and D. G. Pérez, Opt. Lett. **40**, 3145 (2015).
7. D. Gulich, G. Funes, L. Zunino, D. G. Pérez, and M. Garavaglia, Opt. Commun. **277**, 241 (2007).
8. L. C. Andrews, R. L. Phillips, and C. Y. Hopen, *Laser Beam Scintillation with Applications*, Vol. PM99 of SPIE Press Monograph (SPIE, 2001).
9. D. Gulich, G. Funes, D. Pérez, and L. Zunino, Opt. Lett. **40**, 5642 (2015).
10. C.-K. Peng, S. V. Buldyrev, S. Havlin, M. Simons, H. E. Stanley, and A. L. Goldberger, Phys. Rev. E **49**, 1685 (1994).
11. D. Grech and Z. Mazur, Physica A **392**, 2384 (2013).
12. R. Barille and P. LaPenna, Appl. Opt. **45**, 3331 (2006).
13. N. Das, S. Chatterjee, J. Soni, J. Jagtap, A. Pradhan, T. K. Sengupta, P. K. Panigrahi, I. A. Vitkin, and N. Ghosh, Opt. Lett. **38**, 211 (2013).
14. G. Funes, E. Figueroa, D. Gulich, L. Zunino, and D. G. Pérez, Proc. SPIE **8890**, 889016 (2013).
15. L. Zunino, D. Gulich, G. Funes, and A. Ziad, Opt. Lett. **39**, 3718 (2014).

16. J. W. Kantelhardt, E. Koscielny-Bunde, H. H. A. Rego, S. Havlin, and A. Bunde, Physica A **295**, 441 (2001).
17. J. W. Kantelhardt, S. A. Zschiegner, E. Koscielny-Bunde, S. Havlin, A. Bunde, and H. E. Stanley, Physica A **316**, 87 (2002).
18. D. Gulich and L. Zunino, Physica A **397**, 17 (2014).
19. J. Feder, *Fractals* (Plenum, 1988), Chap. 9.
20. M. Charnotskii, Opt. Eng. **52**, 046001 (2013).
21. J. R. Parker, *Algorithms for Image Processing and Computer Vision*, 2nd ed. (Wiley, 2011).
22. A. Fuchs, J. Vernin, and M. Tallon, Appl. Opt. **35**, 1751 (1996).
23. O. Keskin, L. Jolissaint, and C. Bradley, Appl. Opt. **45**, 4888 (2006).
24. E. Masciadri and J. Vernin, Appl. Opt. **36**, 1320 (1997).